

Studies of Quantum-Mechanical Coherency Effects in Neutrino-Nucleus Elastic Scattering

V. Sharma,^{1,2} L. Singh,^{1,3} H.T. Wong,^{1,*} M. Agartioğlu,^{4,5} J.-W. Chen,⁶
M. Deniz,⁴ S. Kerman,^{4,†} H.B. Li,¹ C.-P. Liu,⁵ M.K. Singh,^{1,2} and V. Singh^{2,3}

(TEXONO Collaboration)

¹ *Institute of Physics, Academia Sinica, Taipei 11529, Taiwan.*

² *Department of Physics, Institute of Science, Banaras Hindu University, Varanasi 221005, India.*

³ *Department of Physics, School of Physical and Chemical Sciences, Central University of South Bihar, Gaya 824236, India*

⁴ *Department of Physics, Dokuz Eylül University, Buca, İzmir 35160, Turkey.*

⁵ *Department of Physics, National Dong Hwa University, Shoufeng, Hualien 97401, Taiwan.*

⁶ *Department of Physics, CTS and LeCosPA, National Taiwan University, Taipei 10617, Taiwan.*

(Dated: October 15, 2020)

Neutrino-nucleus elastic scattering provides a unique laboratory to study the quantum-mechanical coherency effects in electroweak interactions. The deviations of the cross-sections from those of completely coherent systems can be quantitatively characterized through a coherency parameter $\alpha(q^2)$. The relations between α and the underlying nuclear physics in terms of nuclear form factors are derived. The dependence of cross-sections on $\alpha(q^2)$ for the various neutrino sources are presented. The $\alpha(q^2)$ -values are evaluated from the measured data of the COHERENT CsI and Ar experiments. Complete coherency and decoherency conditions are excluded by the CsI data with $p=0.025$ at $q^2=3.5\times 10^3$ MeV² and with $p=0.012$ at $q^2=2.6\times 10^3$ MeV², respectively.

PACS numbers: 13.15.+g, 03.65.-w, 21.10.Ft

Keywords: Neutrino Interactions, Quantum Mechanics, Nuclear Form Factors

I. INTRODUCTION

The elastic scattering of a neutrino with a nucleus [1, 2]

$$\nu A_{el}: \quad \nu + A(Z, N) \rightarrow \nu + A(Z, N) \quad , \quad (1)$$

where $A(Z, N)$ denotes the atomic nucleus with its respective atomic, charge and neutron numbers, is a fundamental electroweak neutral current process in the Standard Model (SM).

Studies of neutrino-nucleus elastic scattering can provide sensitive probes to physics beyond SM (BSM) [3, 4] and certain astrophysical processes [1, 5]. It offers prospects to study quantum-mechanical coherency effects in electroweak interactions [6], neutron density distributions [7], to detect supernova neutrinos [8] and to provide a compact and transportable neutrino detectors for real-time monitoring of nuclear reactors [9]. The νA_{el} events from solar and atmospheric neutrinos are the irreducible “neutrino floor” background [10] to forthcoming generations of dark matter experiments [11].

There are active experimental programs to observe and measure the processes with neutrinos from reactors [12] or from decay-at-rest pions (DAR- π) [4] with spallation neutron source [13]. Future dark matter experiments may also be sensitive to νA_{el} from solar neutrinos [14]. First positive measurement of νA_{el} was achieved by the COHERENT experiment with CsI(Na) detector [15], followed by measurements with liquid Ar detector [16].

The νA_{el} reaction provides a laboratory to probe the quantum-mechanical coherency effects [6]. Experimental measurements are mostly performed in parameter space where the coherency effects are partial and incomplete. The deviations from perfect coherency would have to be characterized before this interaction can be effectively applied towards other goals like the studies of BSM physics. Our earlier work [6] identified a coherency parameter $\alpha(q^2)$ which can consistently characterize the transitions between coherent and decoherent states in νA_{el} with different ν -sources and target nuclei. This article follows and expands on these studies. The relations between $\alpha(q^2)$ with the complementary descriptions in terms of nuclear physics with the language of nuclear form factors or with the measurable suppression in cross-sections are discussed in Section II. The dependence of coherency effects with interaction kinematics for various neutrino sources and detector targets are surveyed in Section III. The constraints provided by the COHERENT-CsI [15] and -Ar [16] data are derived in Section IV.

II. FORMULATION AND CHARACTERIZATION

The differential cross-section of νA_{el} scattering at three-momentum transfer q ($\equiv |\vec{q}|$) and neutrino energy E_ν can be expressed as [2, 6]:

$$\left[\frac{d\sigma}{dq^2}(q^2, E_\nu) \right]_{\nu A_{el}} = \frac{1}{2} \left[\frac{G_F^2}{4\pi} \right] \cdot \left[1 - \frac{q^2}{4E_\nu^2} \right] \cdot \Gamma(q^2) \quad , \quad (2)$$

where $\Gamma(q^2)$ is a function describing the contributions due to many-body physics in the target nuclei, since the νA_{el}

*Corresponding Author: htwong@phys.sinica.edu.tw

†Deceased

interactions involve collective contributions of individual nucleons in the nucleus.

The relevant kinematics variable is q^2 which characterizes the physics and is universal to all target. The experimental observable is the nuclear recoil energy (T), expressed in units of keV_{nr} in this article, which depends on the target nuclear mass M and is related to q^2 via $q^2=2MT+T^2\approx 2MT$. The minimal observable energy T_{min} for the nuclear recoils is the detector threshold, while kinematics limits the maximum recoil energy to be $T_{\text{max}}=2E_\nu^2/(M+2E_\nu)\approx 2E_\nu^2/M$. These limits can be translated to $q_{\text{min}}^2=2MT_{\text{min}}$ and $q_{\text{max}}^2=4E_\nu^2[M/(M+2E_\nu)]\approx 4E_\nu^2$. The variations of the νA_{el} differential and integral cross-sections with respect to T are discussed in Appendix A.

Depending on the particular physics aspects to probe, there are complementary formulations on the $\Gamma(q^2)$ function. The usual description is based on nuclear physics, in which

$$\Gamma(q^2) \equiv \Gamma_{NP}(q^2) = [\varepsilon Z F_Z(q^2) - N F_N(q^2)]^2 \quad (3)$$

where $F_Z(q^2)\in[0,1]$ and $F_N(q^2)\in[0,1]$ are, respectively, the proton and neutron nuclear form factors for the nucleus $A(Z, N)$, while $\varepsilon\equiv(1-4\sin^2\theta_W)\approx 0.045$, indicating the dominant contributions are from the neutrons.

The merit of this description is to connect νA_{el} to nuclear physics so that its studies may benefit from or contribute to the wealth of information and data. Electron-nucleus scattering experiments provide important data to the nuclear proton form factor $F_Z(q^2)$ [17]. The neutron counterpart $F_N(q^2)$, however, would require weak processes to probe. Studies of νA_{el} have therefore triggered intense activities towards their measurements [7], complementing experiments with parity-violation scattering using polarized electrons [18].

In the kinematics regime relevant to this work – $q^2 R^2 \ll \pi^2$ (natural units with $\hbar=c=1$ are used throughout), where $R=1.2A^{1/3}$ fm is the typical scale characterizing the radius of nuclei – nucleons can be taken as structureless point-like particles, such that their internal dynamics and QCD effects can be neglected. At $q^2\rightarrow 0$, there is a perfect alignment of the scattering amplitude vectors of individual nucleons in the target nucleus [6]. The interactions are completely coherent. As q^2 increases, deviations from this complete coherency condition lead to suppression in the cross-section. The loss of coherency can be described by a parameter $\alpha(q^2)\equiv\cos\phi\in[0,1]$ where $\phi(q^2)\in[0,\pi/2]$ is the misalignment phase angle [6]. This leads to a formulation in terms of quantum-mechanical coherency among the various scattering centers, in which:

$$\begin{aligned} \Gamma(q^2) &\equiv \Gamma_{QM}(q^2) \\ &= Z\varepsilon^2 [1+\alpha(Z-1)] + N [1+\alpha(N-1)] - 2\alpha\varepsilon ZN \\ &= (\varepsilon Z - N)^2 \cdot \alpha(q^2) + (\varepsilon^2 Z + N) \cdot [1 - \alpha(q^2)] . \end{aligned} \quad (4)$$

The Γ_{QM} -formulation with $\alpha(q^2)$ provides an intuitive physics understanding and quantitative description on

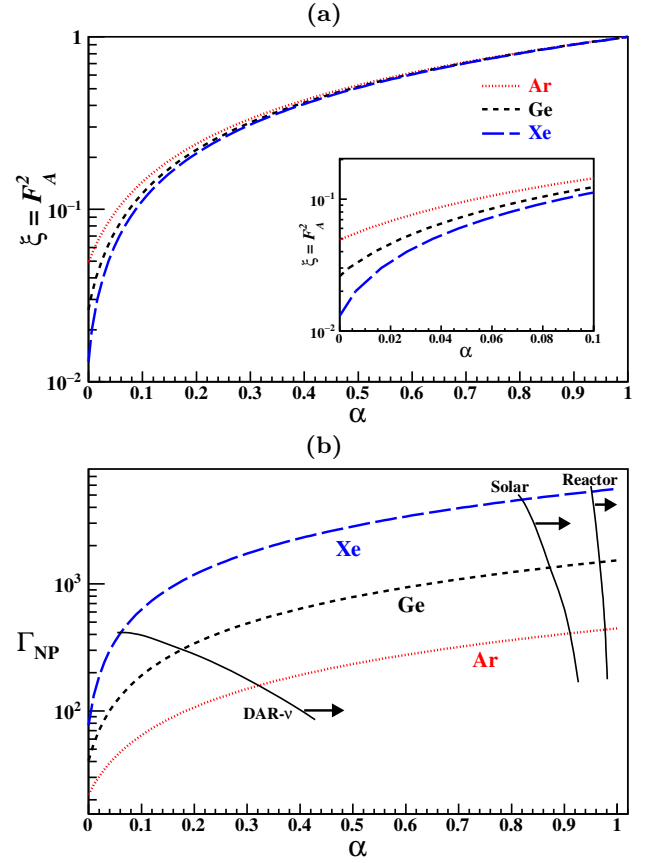


FIG. 1: The variations with α for (a) cross-section ratios ξ (equivalently F_A) and (b) Γ_{NP} for the three target nuclei, independent of underlying nuclear physics. Superimposed in (b) are contours of maximum- q^2 for reactor, solar and DAR- π neutrinos. The limiting values are $\xi=1$ and $\Gamma_{NP}=(\varepsilon Z-N)^2$ at $\alpha=1$ and $\xi=(\varepsilon^2 Z+N)/(\varepsilon Z-N)^2$ and $\Gamma_{NP}=(\varepsilon^2 Z+N)$ at $\alpha=0$.

the suppression of νA_{el} cross-sections in terms of phase-angle alignment and quantum-mechanical coherency. In particular, it naturally leads to the limiting behavior at the complete coherency ($\alpha=1$ at $q^2\sim 0$) and decoherency ($\alpha=0$ at $q^2\gtrsim[\pi/R]^2$) states, corresponding to $(d\sigma/dq^2)\propto[\varepsilon Z - N]^2$ and $(d\sigma/dq^2)\propto[\varepsilon^2 Z + N]$, respectively. The experimentally measured $\alpha(q^2)$ -values from different isotope targets can be directly compared to reveal their varying degrees of coherency in the respective processes.

An alternative measurement-driven description, denoted by $\xi(q^2)$, is the cross-section reduction relative to that of complete coherency condition [6], where

$$\Gamma(q^2) \equiv \Gamma_{DATA}(q^2) = (\varepsilon Z - N)^2 \cdot \xi(q^2) . \quad (5)$$

The functions Γ_{NP} , Γ_{QM} and Γ_{DATA} are complementary descriptions of the νA_{el} interactions. The experimentally measurable cross-section suppression (ξ in Γ_{DATA}) is related to nuclear form factors and quantum-mechanical

TABLE I: Summary of the three formulations which characterize the many-body physics in νA_{el} , and the values of the key parameters at the limiting domains where the scattering amplitudes are either completely in phase (“Coherency”) or decoupled (“Decoherency”).

Conditions	Complete Coherency	Complete Decoherency
q^2	$\rightarrow 0$	$\gtrsim \left[\frac{\pi}{R}\right]^2$ with A -Dependence
(I) $\Gamma_{NP}(q^2) = [\varepsilon Z F_Z(q^2) - N F_N(q^2)]^2$		
$F_Z(q^2)$	1	—
$F_N(q^2)$	1	—
$\Gamma_{NP}(q^2)$	$(\varepsilon Z - N)^2$	$(\varepsilon^2 Z + N)$
(II) $\Gamma_{QM}(q^2) = (\varepsilon Z - N)^2 \alpha(q^2) + (\varepsilon^2 Z + N) [1 - \alpha(q^2)]$		
$\phi(q^2)$	0	$\pi/2$
$\alpha(q^2)$	1	0
(III) $\Gamma_{DATA}(q^2) = (\varepsilon Z - N)^2 \xi(q^2)$		
$\xi(q^2)$	1	$\left[\frac{(\varepsilon^2 Z + N)}{(\varepsilon Z - N)^2}\right]$
$\left[\frac{d\sigma}{dq^2}\right](q^2)$	$\propto (\varepsilon Z - N)^2$	$\propto (\varepsilon^2 Z + N)$

coherency (α in Γ_{QM}) via, respectively,

$$\xi(q^2) = \alpha(q^2) + [1 - \alpha(q^2)] \left[\frac{(\varepsilon^2 Z + N)}{(\varepsilon Z - N)^2} \right] \quad (6)$$

and

$$\xi(q^2) = \frac{[\varepsilon Z F_Z(q^2) - N F_N(q^2)]^2}{(\varepsilon Z - N)^2}, \quad (7)$$

while the two physics descriptions are connected by:

$$[\varepsilon Z F_Z(q^2) - N F_N(q^2)]^2 = (\varepsilon Z - N)^2 \cdot \alpha(q^2) + (\varepsilon^2 Z + N) \cdot [1 - \alpha(q^2)]. \quad (8)$$

The relations between ξ and Γ_{NP} with α for three representative nuclei are shown in Figures 1a&b, respectively. Contours of maximum- q^2 for different neutrino sources are marked in Figure 1b. The behavior of Γ_{NP} , α and ξ at the limiting domains corresponding to the complete coherency and decoherency conditions are summarized in Table I. In particular, the relation $\Gamma_{NP} = (\varepsilon^2 Z + N)$ for completely decoherent νA_{el} interactions is a result that emerges by relating Γ_{NP} and Γ_{QM} in Eq. 8, and could not be derived by considerations of nuclear form factor of Eq. 3 alone.

III. PROJECTED EXPERIMENTAL RANGES

The functions Γ_{NP} , Γ_{QM} and Γ_{DATA} can be directly measured from νA_{el} data without input from the underlying

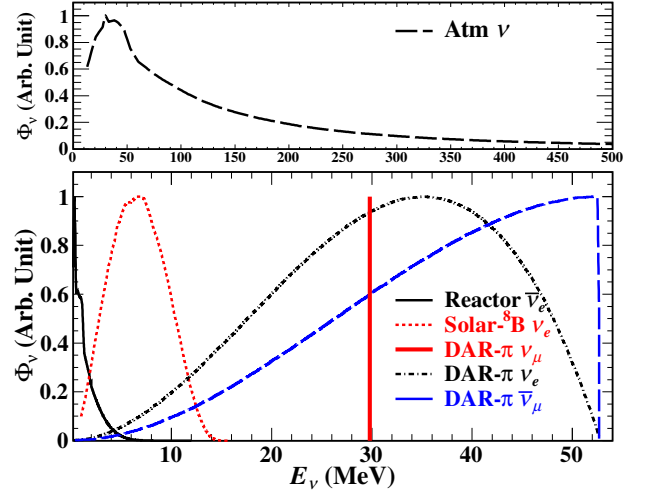


FIG. 2: Neutrino spectra (Φ_ν) from (top) atmospheric as well as (bottom) reactor $\bar{\nu}_e$, solar ${}^8\text{B}$ ν_e and DAR- π (ν_μ , ν_e , $\bar{\nu}_\mu$) neutrinos adopted from Ref. [21] and normalized by their maxima.

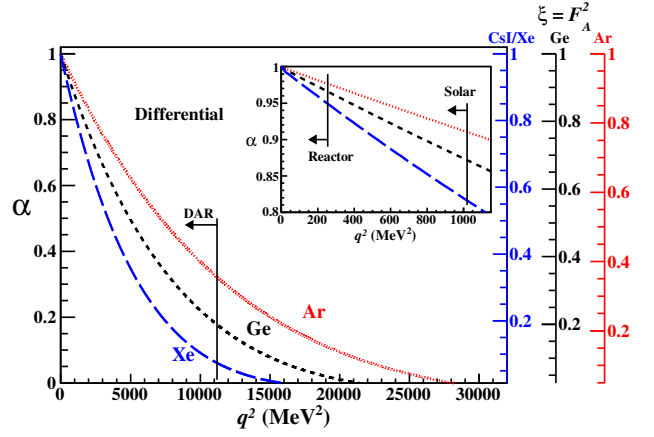


FIG. 3: The variation of α and $\xi (= F_A^2)$ as a function of q^2 of νA_{el} on the three selected nuclei. Different neutrino sources share the same contour for the same target in q^2 -space, but with different ranges. The end-points for reactor, solar and DAR- π neutrinos are marked.

physics. Prior to actual measurements, specific formulations of the nuclear form factors have to be adopted for phenomenological studies and to establish the typical ranges to guide the choices of experimental parameters. To serve these purposes, the frequently adopted approach is to take the nuclear form factors for protons and neutrons are identical: $F_N(q^2) = F_Z(q^2) \equiv F_A(q^2)$, and to use the effective “Helm Form Factor” description of Ref. [20]:

$$F_A(q^2) = \left[\frac{3}{qR_0} \right] j_1(qR_0) \exp \left[-\frac{1}{2} q^2 s^2 \right], \quad (9)$$

where $j_1(x) = [(\sin x/x^2) - (\cos x/x)]$ is the first-order spherical Bessel function. The nuclear dependence appears through $R_0^2 = R^2 - 5s^2$, where $s = 0.5$ fm is the surface

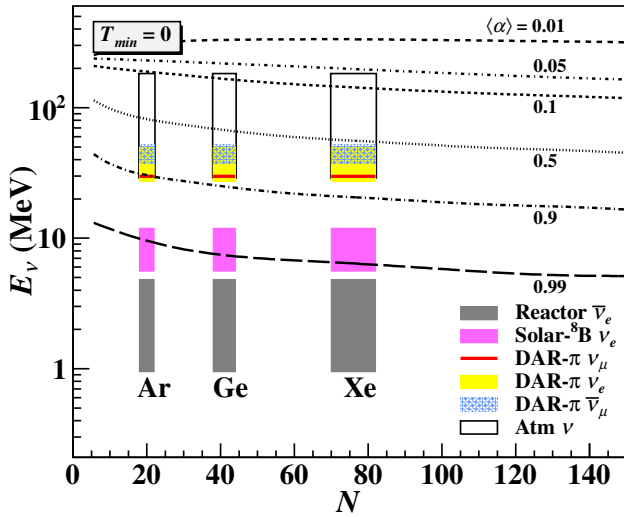


FIG. 4: The contours of the mean degree of coherency $\langle \alpha \rangle$ on the (N, E_ν) plane at $T_{min}=0$, with bands of neutrino sources and target nuclei superimposed. The ranges in E_ν correspond to FWHM in $[\Phi_\nu \cdot \sigma_{\nu A_{el}}]$.

thickness of the nuclei. In this formulation, the squared-form factor is equivalent to the cross-section suppression fraction: $[F_A(q^2)]^2 = \xi(q^2)$.

Typical spectra [21] of reactor, solar and atmospheric neutrinos, as well as those due to decay-at-rest π (DAR- π), are used in this study. These are depicted in Figure 2.

The measurable total cross-section is given by convoluting Eq. 2 with the neutrino spectrum $\Phi_\nu(E_\nu)$, and integrating over E_ν and $q^2 \in [q_{min}^2, q_{max}^2]$, from which the mean suppression fraction $\langle \xi \rangle$ and the mean coherency factor $\langle \alpha \rangle$ can be derived [19].

The νA_{el} processes on several nuclei of experimental interest and at different mass ranges are studied – (Ar;Ge;Xe) with $Z=(18;32;54)$. The target that provides the first νA_{el} measurements [15] – CsI, having $Z=55$ and 53, respectively, can be approximated as Xe in this discussion.

The variations of α and $\xi(=F_A^2)$ with q^2 of the four neutrino sources, with three selected nuclei (Ar;Ge;Xe) are depicted in Figure 3. The q^2 -dependence is universal for the different neutrino sources, though their q_{max}^2 -values are distinct due to their varying maximum E_ν . These spectra end-points for reactor, solar and DAR- π neutrinos are well-defined, and their corresponding ranges in α and q^2 are depicted in Figures 1b&3, respectively.

A summary plot on the variations of $\langle \alpha \rangle$ with the neutrino sources and target nuclei is illustrated in Figure 4, in which the ranges in E_ν are defined by the Full-Width-Half-Maximum (FWHM) of $[\Phi_\nu \cdot \sigma_{\nu A_{el}}]$. For completeness, the differential and integral event rates due to the four neutrino sources in measurable nuclear recoil energy T , together with their corresponding α and $\langle \alpha \rangle$ values, are discussed and presented in Appendix A.

It can be seen that coherency is mostly complete

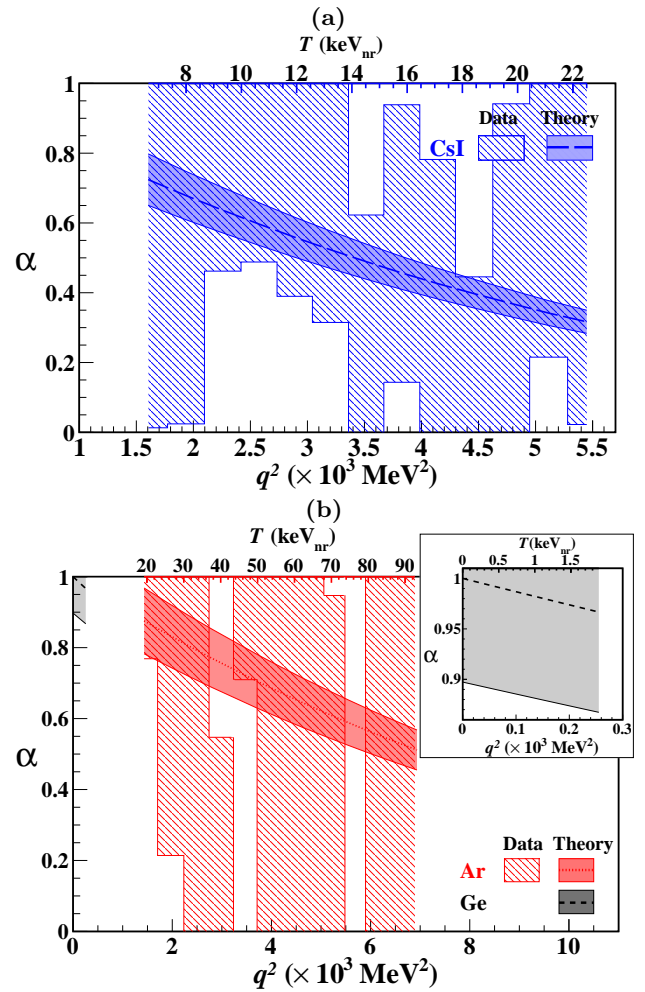


FIG. 5: Measurements on α from COHERENT (a) CsI [15] and (b) Ar [16] data with DAR- π - ν . The stripe-shaded areas are the 1- σ allowed regions derived from the reduction in cross-section relative to the complete coherency conditions independent of nuclear physics input. The dark-shaded regions are the theoretical expectations adopting the nuclear form factor formulation of Eq. 9 with a $\pm 1\sigma$ uncertainty of 10%. The same projection applies to reactor- ν on Ge in (b) with q^2 -range specified by FWHM in $[\Phi_\nu \cdot \sigma_{\nu A_{el}}]$. The $\alpha(q^2)$ -values for different nuclei can be consistently compared.

($\alpha > 95\%$) for νA_{el} with reactor and solar neutrinos, whereas coherency is only partial for DAR- π and weak for atmospheric neutrinos. Accordingly, studies of νA_{el} with different neutrino sources provide complementary information and cover the transitions from completely coherent to decoherent states.

IV. MEASUREMENTS FROM CURRENT DATA

The COHERENT-CsI(Na) [15] and -Ar [16] experiments at the DAR- π beam with the Spallation Neutron Source facility at the Oak Ridge National Laboratory provide positive measurements on νA_{el} .

TABLE II: Averaged $[\langle\alpha\rangle; \langle\xi\rangle]$ and total event rates in $\text{kg}^{-1}\text{day}^{-1}$ for the target nuclei at a threshold of 1 and 10 keV_{nr} and for different ν -sources. Reactor and DAR- π neutrino fluxes are taken to be $10^{13} \text{ cm}^{-2}\text{s}^{-1}$, while DAR- π neutrino flux is $3.4 \times 10^{14} \text{ cm}^{-2}\text{yr}^{-1}$ /flavor at 19.3 m from target at beam intensity $2 \times 10^{23} \text{ POT yr}^{-1}$. Rates due to atmospheric neutrinos are from the integration of q^2 -ranges corresponding to $\alpha \in [0.01, 1.0]$.

Detector Target	ν -Sources			
	DAR- π	Reactor	Solar	Atmospheric
	$[\langle\alpha\rangle; \langle\xi\rangle]$		$[\langle\alpha\rangle; \langle\xi\rangle]$	
	Total Event Rates ($\text{kg}^{-1}\text{yr}^{-1}$)		Total Event Rates ($\text{ton}^{-1}\text{yr}^{-1}$)	
	Detector Threshold = 1 keV_{nr}			
Ar	[0.92 ; 0.93] 27.2	[0.99 ; 0.99] 766	[0.98 ; 0.98] 130	[0.61 ; 0.63] 0.019
Ge	[0.84 ; 0.84] 46.1	[0.98 ; 0.98] 138	[0.97 ; 0.97] 140	[0.46 ; 0.47] 0.028
Xe	[0.72 ; 0.72] 77.8	[0.95 ; 0.95] 0.07	[0.94 ; 0.94] 95.7	[0.41 ; 0.42] 0.039
	Detector Threshold = 10 keV_{nr}			
Ar	[0.87 ; 0.87] 19.2	N/A	N/A	[0.57 ; 0.59] 0.017
Ge	[0.72 ; 0.72] 22.6	N/A	N/A	[0.37 ; 0.39] 0.022
Xe	[0.46 ; 0.47] 17.1	N/A	N/A	[0.24 ; 0.25] 0.021

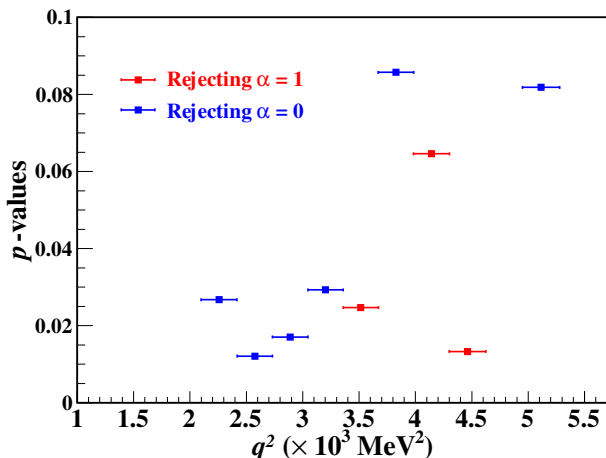


FIG. 6: The p -value significance to probe the specific cases corresponding to the complete coherency ($\alpha=1$, in red) and decoherency ($\alpha=0$, in blue) conditions from the COHERENT-CsI data [15].

While the first-generation “discovery” measurements cannot be expected to provide severe constraints on $\alpha(q^2)$, it is instructive to go through the data analysis to establish the ranges of the effects and to check consistency. Values and uncertainties of $\alpha(q^2)$ are derived from the measured spectra and displayed in Figures 5a&b for CsI and Ar, respectively.

The bin-wise $\xi(q^2)$ cross-section suppression relative to the complete coherency condition was provided by measurements. The allowed $1\text{-}\sigma$ ranges in $\alpha(q^2)$ are evaluated

according to Eq. 6 and depicted as stripe-shaded regions in Figures 5a&b. The results are data-driven without invoking nuclear physics input. The theoretical expectations adopting the nuclear form factor formulation of Eq. 9 with a $\pm 1\sigma$ uncertainty of 10% are superimposed as dark-shaded bands, showing the cases with CsI (equivalently, Xe) and Ar at DAR- π , and with Ge at reactors.

It can be seen that the current data are consistent with the predictions from Eq. 9. Future measurements with sufficient accuracies would probe the transitions in quantum-mechanical coherency according to:

$$\begin{aligned}
 &\text{CsI/Xe @ DAR-}\pi : \\
 &\quad \alpha \in [0.72, 0.32] \text{ for } T \in [6, 23] \\
 &\text{Ar @ DAR-}\pi : \\
 &\quad \alpha \in [0.88, 0.51] \text{ for } T \in [19, 93] \\
 &\text{Ge @ Reactor :} \\
 &\quad \alpha \in [1.00, 0.97] \text{ for } T \in [0, 1.9] ,
 \end{aligned} \tag{10}$$

following the T -ranges used in Figure 5.

The significance in terms of p -values of the CsI data in probing the specific cases of complete coherency(decoherency) at $\alpha=1(0)$ are depicted in Figures 6. Independent of nuclear physics input, the complete coherency and decoherency conditions are excluded with $p=0.025$ at $q^2=3.5 \times 10^3 \text{ MeV}^2$ and with $p=0.012$ at $q^2=2.6 \times 10^3 \text{ MeV}^2$, respectively.

These diverse ranges of α -sensitivity indicate the complementarity of νA_{el} measurements among reactor and DAR- π -neutrinos. Future measurements of solar νA_{el} [14] with multi-ton detectors would probe a similar

range of α as reactor neutrinos. Xenon detectors with scale $\mathcal{O}(100)$ ton would be required to probe the weakly-coherent region at $\alpha < 0.2$ with atmospheric neutrinos.

V. SUMMARY AND PROSPECTS

Neutrino-nucleus elastic scattering provides a laboratory to study quantum-mechanical coherency effects in electroweak interactions. This interpretation of the process is complementary to the language of nuclear form factors describing the nucleon-nucleus interplay.

We relate the two approaches in this work. Current positive measurements on νA_{el} provide weak constraints to the coherency-parameter $\alpha(q^2)$. Data with $\mathcal{O}(10\%)$ accuracy would allow the studies of coherency transitions over a large range of α .

We note that the interaction νA_{el} of Eq. 1 involves two distinct concepts: elastic kinematics and quantum-mechanical coherency. The coherency aspect should be characterized by distributions with dependence on $A(Z, N)$ and q^2 . Descriptions of coherency as a binary state or having both concepts bundled together may have the unintended consequences of missing the complexities of the process and suppressing the potential richness of its physics content.

VI. ACKNOWLEDGEMENT

This work is supported by the Academia Sinica Principal Investigator Award AS-IA-106-M02, Contracts 106-2923-M-001-006-MY5, 107-2119-M-001-028-MY3 and 109-2112-M-259-001 from the Ministry of Science and Technology, Taiwan, and 2017-ECP2 from the National Center of Theoretical Sciences, Taiwan. This article is dedicated to the memory of Dr. Saime Ker-man.

Appendix A: Measurable Event Rates

The differential cross-section of Eq. 2 on q^2 can be translated to one on measurable nuclear recoil-energy T by

$$\left[\frac{d\sigma}{dT} \right]_{\nu A_{el}} = 2M \left[\frac{d\sigma}{dq^2} \right]_{\nu A_{el}}. \quad (\text{A1})$$

The measurable differential spectra (dR/dT) convoluted with the neutrino spectrum $\Phi_\nu(E_\nu)$ is given by:

$$\left(\frac{dR}{dT} \right)_{\nu A_{el}} = 2M \int \left[\left(\frac{d\sigma}{dq^2} \right)_{\nu A_{el}}(T, E_\nu) \right] \Phi_\nu(E_\nu) dE_\nu. \quad (\text{A2})$$

Integration over $T \in [T_{min}, T_{max}]$ gives the total event rates.

The universality of Figure 3 no longer applies when q^2 is replaced by T . The variations of α , F_A and ξ with T depend on E_ν -distributions and therefore neutrino sources. The variations are depicted in Figure 7.

The differential rates derived from the four sources and three targets are displayed in Figure 8. The corresponding total rates are shown in Figure 9, showing their variations with T_{min} and $\langle \alpha \rangle$. The values of $\langle \alpha \rangle$ and $\langle \xi \rangle$ as well as the total event rates at $T_{min}=1(10)$ keV_{nr} for the various neutrino sources and target nuclei are summarized in Table II. Evaluation of these rates are based on standard solar and atmospheric spectra [21]. Reactor $\bar{\nu}_e$ flux is taken to be 10^{13} cm⁻²s⁻¹, while DAR- π per-flavor neutrino flux is 3.4×10^{14} cm⁻²yr⁻¹ corresponding to 2×10^{23} proton-on-target(POT)/year at 19.3 m from target [15]. There is no high-energy cut-off in E_ν for the atmospheric neutrino spectra. The differential and integral spectra of Figures 8&9d are therefore evaluated for $\alpha \in [0.01, 1.0]$, corresponding to $T < (361; 148; 60)$ keV_{nr} for (Ar; Ge; Xe).

Typically, measurements of νA_{el} with reactor and solar neutrinos require $\mathcal{O}(1)$ keV_{nr} detector threshold giving expected rates of $\mathcal{O}(1)$ /kg-day and $\mathcal{O}(1)$ /ton-yr, respectively. The corresponding event rates for DAR- π and atmospheric neutrinos are $\mathcal{O}(10)$ /kg-yr and $\mathcal{O}(0.01)$ /ton-yr at a threshold of $\mathcal{O}(10)$ keV_{nr}, respectively.

At the detection threshold of 1 keV_{nr}, 90% of the elastic scattering events between Weakly Interacting Massive Particles (WIMPs)-dark matter of mass 1 TeV with (Ar; Ge; Xe)-target have recoil energy up to (99; 74; 35) keV_{nr}. These kinematics ranges correspond to α as low as (0.49; 0.22; 0.14) for νA_{el} scattering with atmospheric neutrinos, as indicated in Figure 7d – far from the complete coherency regime. Accordingly, the description of “the neutrino floor originates from *coherent* neutrino-nucleus scattering” is not applicable for WIMPs at TeV or higher mass scales.

-
- [1] D.Z. Freedman, Phys. Rev. **D 9**, 1389 (1974); D.Z. Freedman, D.N. Schramm, and D.L. Tubbs. Ann. Rev. Nil. Part. Sci. **27**, 167 (1977).
[2] D.K. Papoulias and T.S. Kosmas, Adv. High Energy Phys. **2015**, 763648 (2015).
[3] L.M. Krauss, Phys. Lett. **B 269**, 407 (1991); J. Barranco,

- O.G. Miranda and T.I. Rashba, JHEP. **12**, 021 (2005); J. Barranco, O.G. Miranda and T.I. Rashba, Phys. Rev. **D 76**, 073008 (2007); D.K. Papoulias et al., Front. Phys. **7**, 191 (2019).
[4] K. Scholberg, Phys. Rev. **D 73**, 033005 (2006).
[5] J.R. Wilson, Phys. Rev. Lett. **32**, 849 (1974).

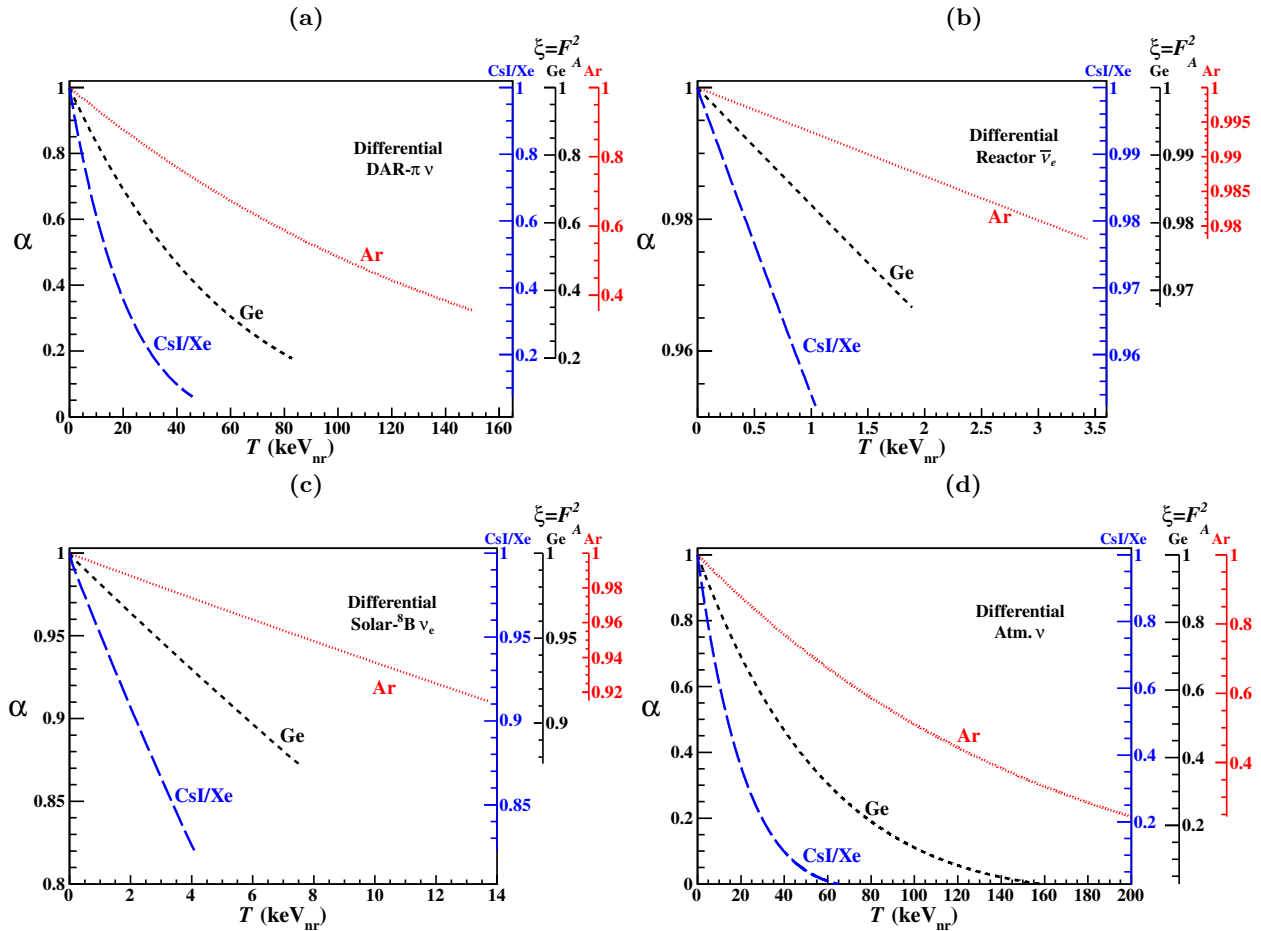


FIG. 7: The variations of α and $\xi(=F_{\lambda}^2)$ with T in νA_{el} on the three selected nuclei for (a) DAR- π , (b) Reactor, (c) Solar, and (d) Atmospheric neutrinos.

- [6] S. Kerman et al., Phys. Rev. **D 93**, 113006 (2016).
- [7] K. Patton et al., Phys. Rev. **C 86**, 024612 (2012); E. Ciuffoli et al., Phys. Rev. **D 97**, 113003 (2018); M. Cadeddu et al., Phys. Rev. Letts. **120**, 072501 (2018); D.A. Sierra et al., J. High Energy Phys. **2019**, 141 (2019). C.G. Payne, Phys. Rev. **C 100**, 061304(R) (2019); P. Coloma et al., arXiv:2006.08624 (2020).
- [8] C.J. Horowitz, K.J. Coakley, and D.N. McKinsey, Phys. Rev. **D 68**, 023005 (2003).
- [9] J. Learned, Nucl. Phys. B (Proc. Suppl.) **143**, 152 (2005).
- [10] J. Monroe and P. Fisher, Phys. Rev. **D 76**, 033007 (2007); A. Gütlein et al., Astropart. Phys. **34**, 90 (2010); J. Billard, E. Figueroa-Feliciano, and L. Strigari. Phys. Rev. **D 89**, 023524 (2014).
- [11] M. Drees and G. Gerbier, Review of Particle Physics Phys. Rev. **D 98**, 030001:396 (2018), and references therein.
- [12] H.T. Wong et al., J. Phys. Conf. Ser. **39**, 266 (2006); V. Belov et al., J. Instrum. **10**, P12011 (2015); G.F. Moroni et al., Phys. Rev. **D 91**, 072001 (2015); A.K. Soma et al., Nucl. Instrum. Meth. **A 836**, 67 (2016); G. Agnolet et al., Nucl. Instrum. Meth. **A 853**, 53 (2017); C. Buck et al., J. Phys. Conf. Ser. 1324.012094 (2020); J. Roth et al., J. Low Temp. Phys. **199**, 433 (2020).
- [13] F.T. Avignone and Yu.V. Efremenko, J. Phys. **G 29**, 2615 (2003); D. Akimov et al., arXiv:1509.08702 (2015) and references therein for current experimental projects.
- [14] L.E. Strigari et al., New J. Phys. **11**, 105011 (2009); L. Baudis et al., J. Cos. Astropart. Phys. 01, 044 (2014).
- [15] J.I. Collar et al., Nucl. Instrum. Meth. **A 773**, 56 (2015); D. Akimov et al., Science **357**, 1123 (2017); J.I. Collar et al., Phys. Rev. **D 100**, 033003 (2019).
- [16] D. Akimov et al., Phys. Rev. **D 100**, 115020 (2019); D. Akimov et al., arXiv:2003.106302 (2020).
- [17] I. Angeli and K.P. Marinova, At. Data Nucl. Data Tables **99**, 69 (2013); J.E. Amaro et al., arXiv 1912.1061 (2019).
- [18] T.W. Donnelly, J. Dubach, and I. Sick, Nucl. Phys. **A 503**, 589 (1989);
- [19] The α and ξ results of Ref. [6] are mean values equivalent to $\langle\alpha\rangle$ and $\langle\xi\rangle$, respectively, in this article.
- [20] J. Engel, Phys. Lett. **B 264**, 114 (1991).
- [21] J.N. Bahcall et al., Phys. Rev. Lett. **92**, 121301 (2004); G. Battistoni et al., Astropart. Phys. **23**, 526 (2005); H.T. Wong et al., Phys. Rev. **D 75**, 012001 (2007); D. Akimov et al., Science 10.1126/science.aao0990 (2017).

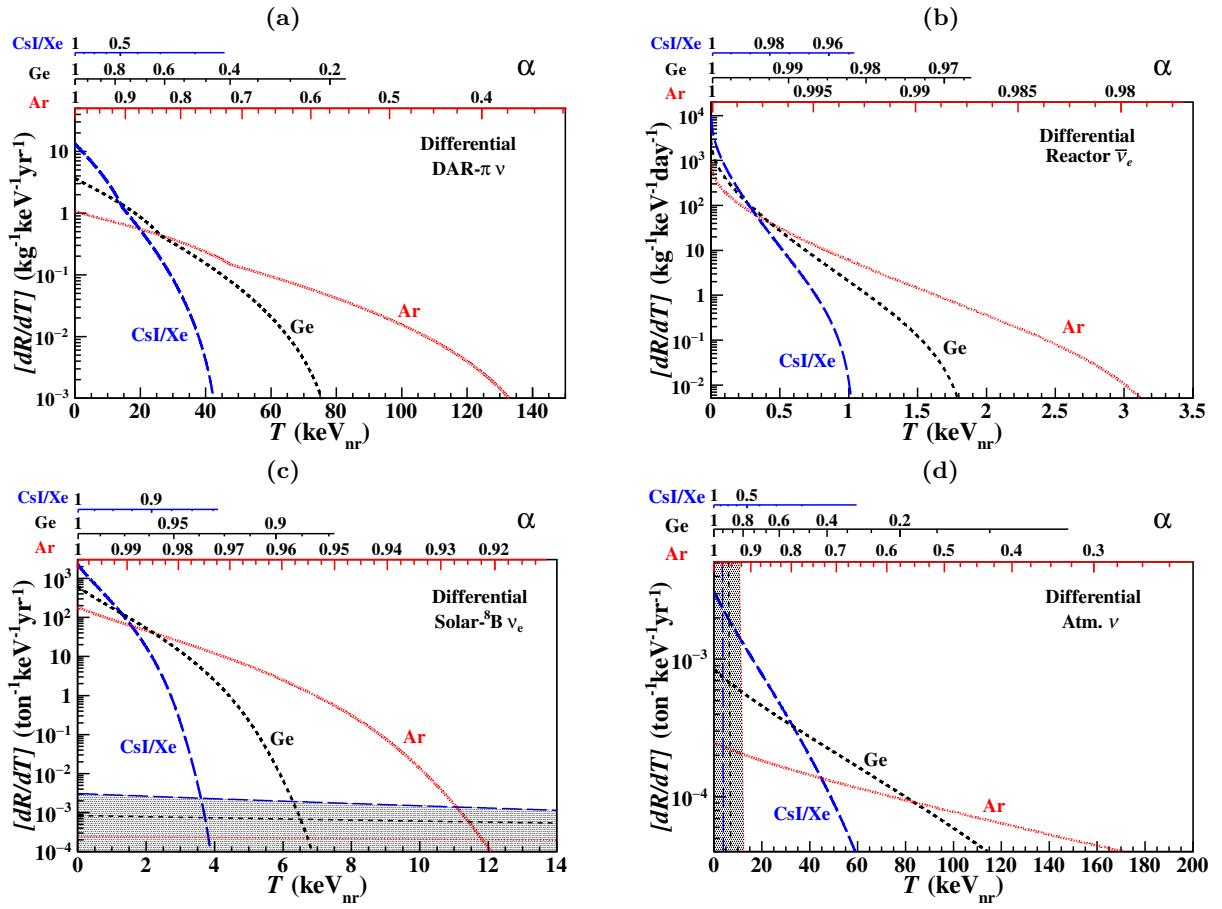


FIG. 8: Differential event rates $[dR/dT]$ of νA_{eI} on the three selected nuclei, and their correlations with α , with (a) DAR- π , (b) Reactor, (c) Solar, and (d) Atmospheric neutrinos. Superimposed as shaded regions in (c) and (d) are the background rates due to atmospheric and solar neutrinos, respectively.

